

A three dimensional object point process for detection of cosmic filaments †

Radu S. Stoica

Université Lille 1, Laboratoire Paul Painlevé, 59655 Villeneuve d'Ascq Cedex, France.

Vicent J. Martínez

Observatori Astronòmic de la Universitat de València, Edifici d'Instituts d'Investigació, Polígon La Coma s/n, 46980 Paterna, València, Spain.

Enn Saar

Tartu Observatoorium, Tõravere, 61602 Estonia

Summary. We propose to apply an object point process to automatically delineate filaments of the large-scale structure in redshift catalogues. We illustrate the feasibility of the idea on an example of the recent 2dF Galaxy Redshift Survey, describe the procedure, and characterise the results.

Keywords: Object point processes, Bisous model, filaments, cosmology, large-scale structure

1. Introduction

The large-scale structure of the Universe traced by the three-dimensional distribution of galaxies shows intriguing patterns: filaments and sheet-like structures connecting in huge clusters surround nearly empty regions, the so-called voids. Surveys of galaxies are created by measuring for each galaxy in addition to its angular position on the sky its distance, estimated from their recession velocities, within the framework of a cosmological model. However, the measured recession velocities are not only due to the Hubble expansion, they appear contaminated by the line-of-sight contribution of the dynamical velocity of a galaxy, due to the local gravitational effects, so the distances of galaxies are in error. Galaxy surveys based on recession velocities are called 'redshift space' maps, and although they are distorted versions of the three-dimensional distribution of galaxies, distance errors are not as serious as to change the overall picture of the large-scale structure.

An overview of such galaxy maps is given in Martínez and Saar (2002). As an example, we present here a map from a recently completed 2dF Galaxy Redshift Survey (2dFGRS, Colless et al. (2001)). This survey measured the redshifts (recession velocities) of galaxies in about 1500 square degrees, up to the distances of about $700 h^{-1} \text{Mpc} \ddagger$ (corresponding to a redshift $z = 0.2$ for the standard cosmological model). The redshifts were measured in two different regions of the sky; Fig. 1 shows the positions of galaxies in two 2.6° thick slices from both regions.

†*Address for correspondence:* Vicent J. Martínez, Observatori Astronòmic de la Universitat de València, Edifici d'Instituts d'Investigació, Polígon La Coma s/n, 46980 Paterna, València, Spain.
E-mail: martinez@uv.es

‡ Distances between galaxies are usually measured in megaparsecs (Mpc); $1 \text{Mpc} \approx 3 \cdot 10^{24} \text{cm}$. The constant h is the dimensionless Hubble parameter; the latest determinations give for its value $h \approx 0.71$.

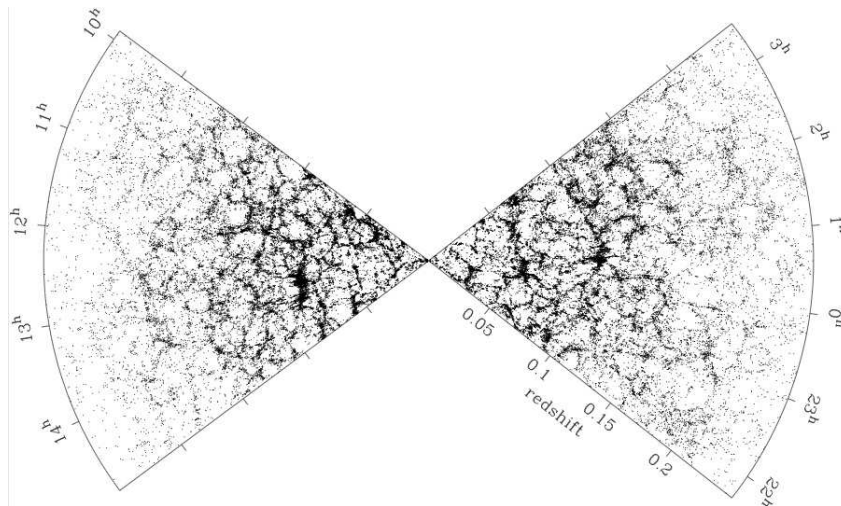


Fig. 1. Galaxy map for two 2dFGRS slices. The observers (we) are situated at the centre of the figure. Both slices are thin, with the thickness of 2.6° . The distances are given in redshifts z ; approximately, the physical distance $D \approx 3000 h^{-1} z$ Mpc. The numbers along the arcs show the right ascension (in hours). The filamentary network of galaxies is clearly seen; the disappearance of structure with depth (towards the sides of the figure) is caused by luminosity selection.

The most characteristic feature of all three-dimensional galaxy cartographies are the remarkable network of filaments that can be appreciated when diagrams like the one shown in Fig. 1 are depicted. All filaments are not equal, they show different size and contrast, but typically relatively empty voids are found between them. Different scales are involved in the filamentary patterns, and it is of great importance to have algorithms to identify them and to characterise their properties. We should mention here that the gradual disappearance of structures with distance observed in Fig. 1 is a selection effect due to how this surveys are built. They are flux-limited samples, and since the apparent luminosity of a galaxy is fainter if the galaxy lies further away, only the brightest galaxies are seen in the more distant regions of the surveyed volume.

Certainly filaments are prominent and visually they dominate the galaxy maps, however there are still no standard methods to describe the observed filamentary structure. Second-order summary statistics like the two-point correlation function, the K -function or the power spectrum (in Fourier space) do not provide morphological information. Minkowski functionals, minimal spanning tree (MST), percolation and shapefinders have been introduced for this purpose (for a review see Martínez and Saar (2002)).

The minimal spanning tree was introduced in cosmology by Barrow et al. (1985). It is a unique graph that connects all points of the process without closed loops, but certainly describes mainly the local nearest-neighbour distribution, being unable to provide a whole characterisation of the global and large-scale properties of the filamentary network.

A better method, named *skeleton*, has been recently proposed (Eriksen et al. (2004); Novikov et al. (2006)) to describe the possible filamentary structure of continuous density fields. The skeleton is determined by segments parallel to the gradient of the field, connecting saddle points to local maxima. Calculating the skeleton involves interpolation and

smoothing the point distribution, which introduces an extra parameter, the band-width of the kernel function used to estimate the density field from the point distribution, typically a Gaussian function. In any case, this method has been recently applied to the Sloan Digital Sky Survey (Sousbie et al. (2006), providing, by means of the length of the skeleton, a good discriminant tool for the analysis of the filamentary structures.

In a previous paper (Stoica et al. (2005b)), we proposed to use an automated method to trace filaments for realisations of point processes, that has been shown to work well for detection of road networks in remote sensing situations (Lacoste et al. (2005); Stoica et al. (2002, 2004)). This method is based on the Candy model, a marked point process where segments serve as marks. The Candy model can be applied to 2-D filaments, and we tested it on simulated galaxy distributions. The filaments we found delineated well the filaments detected by eye.

Many methods used to automatically detect filaments have been developed so far for two-dimensional maps. This is a natural approach for studying the cosmic microwave sky background (Eriksen et al. (2004)), which is two-dimensional, but galaxy maps are three-dimensional. The previous filament studies (e.g., Bharadwaj et al. (2004); Bharadwaj and Pandey (2004); Pandey and Bharadwaj (2005)) have also used two-dimensional galaxy maps, projections for thin slices. The main reason for that is that most of the past large-scale galaxy maps were observed for relatively thin spatial slices; also, in projection filaments seem more prominent. But, of course, both slicing of filaments and projecting the distribution onto a plane distorts the geometry and the properties of the filamentary network.

The study of the three-dimensional filamentary network has just begun. Three-dimensional filaments have been extracted from galaxy distribution as a result of special observational projects (Pimblet and Drinkwater (2004)), or by searching for filaments in the 2dFGRS catalogue (Pimblet et al. (2004)). These filaments have been searched for between galaxy clusters, determining the density distribution and deciding if it is filamentary, individually for every filament. Similar studies have been carried out for N-body simulations (Colberg et al. (2005)). A review of these and previous studies of large-scale filaments is given in (Pimblet (2005)).

No automated methods to trace filaments in the three-dimensional galaxy maps have been proposed so far. Based on our previous experience with the Candy process, we generalised the approach for three dimensions. As the interactions between the structure elements are more complex in three dimensions, we had to define a more complex model, the Bisous model (Stoica et al. (2005a)). This model gives a general framework for the construction of complex patterns made of simple interacting objects. In our case, it can be seen as a generalisation of the Candy model. We will describe the Bisous model below and will apply it to the samples chosen from the real three-dimensional galaxy distribution, the 2dFGRS catalogue.

2. Object point processes: definitions and manipulation tools

2.1. Definitions

Let (K, \mathcal{B}, ν) be a measure space, where K is a compact subset of \mathbb{R}^3 with strictly positive Lebesgue measure $0 < \nu(K) < \infty$ and \mathcal{B} the associated Borel σ -algebra of subsets of K . If, to points in K , shape descriptors or marks are attached, objects are formed. Let (M, \mathcal{M}, ν_M) be the probability measure space of these marks.

The considered configuration space is $\Omega = \cup_{n=0}^{\infty} \Xi_n$, with Ξ_n the set of all unordered

configurations $\mathbf{y} = \{(k_1, m_1), (k_2, m_2), \dots, (k_n, m_n)\}$ that consist of n not necessarily distinct objects $y_i = (k_i, m_i) \in K \times M$. Ξ_0 is the empty configuration. Ω is equipped with the σ -algebra \mathcal{F} generated by the mappings that count the number of objects in Borel sets $A \subseteq K \times M$.

A marked point process with locations of objects in K and marks in M is a measurable mapping from some probability space into (Ω, \mathcal{F}) . An object point process is a marked point process with marks representing shape descriptors of the objects.

For simplicity, throughout this paper the shape of an object is defined by a compact set $s(y_i) = s(k_i, m_i)$ that is a subset of \mathbb{R}^3 of finite volume $\nu(s(y_i))$. The shape of the object configuration \mathbf{y} is defined by the random set $Z(\mathbf{y}) = \cup_{i=1}^{n(\mathbf{y})} s(y_i)$.

The simplest object point process is the Poisson object point process. This process is used as a reference measure. It generates a configuration of objects as follows: first the number of objects is chosen according to a Poisson law of intensity $\nu(K)$, then the locations of objects are distributed uniformly in K and finally the corresponding shapes are chosen independently for each object with respect to ν_M .

The Poisson object point process does not take into account interactions between objects. Indeed, more realistic models can be constructed by specifying a probability density with respect to the reference measure:

$$p(\mathbf{y}|\theta) = \alpha \exp[-U(\mathbf{y}|\theta)] \quad (1)$$

with the normalising constant α , the model parameter vector θ and the energy function of the system $U(\mathbf{y}|\theta)$. There is a lot of freedom for constructing the energy function, provided there exists a positive real constant $\Lambda > 0$ such that

$$U(\mathbf{y}|\theta) - U(\mathbf{y} \cup \{(k, m)|\theta\}) \leq \log \Lambda \quad (2)$$

The condition (2) is known in the literature as the local stability property and it implies the integrability with respect to the reference measure, of the probability density given by (1). Furthermore, the local stability property is of major importance in establishing convergence proofs for the Monte Carlo dynamics simulating such a model Geyer (1999). The quantity $\exp[U(\mathbf{y}|\theta) - U(\mathbf{y} \cup \{(k, m)|\theta\})]$ is usually called the Papangelou or the conditional intensity ratio.

For further details related to the definition and the properties of object point processes we recommend the reader the following monographs (van Lieshout (2000); Møller and Waagepetersen (2003); Reiss (1993)).

2.2. Manipulation tools: sampling and inference

Several Markov chain Monte Carlo Markov techniques are available to simulate object point processes (Geyer and Møller (1994); Geyer (1999); Green (1995); Kendall and Møller (2000); van Lieshout (2000); van Lieshout and Stoica (2006); Preston (1977)).

In this paper, we need to sample from the joint law $p(\mathbf{y}, \theta)$. This is done using an iterative Monte Carlo algorithm. An iteration of the algorithm consists of two steps. First, a parameter value is chosen with respect to $p(\theta)$. Then, conditionally on θ , the pattern is sampled from $p(\mathbf{y}|\theta)$ using a Metropolis-Hastings algorithm (van Lieshout and Stoica (2003a); Stoica et al. (2004, 2005a,b)).

For the problem on hand, \mathbf{d} , the data to be analysed, consist of points (galaxies) spread in a finite volume K . We want to detect the filamentary pattern “hidden” in these data.

Two hypotheses are assumed. First, this rather complex pattern is supposed to be formed by simple interacting objects. Second, the filamentary pattern is considered to be a realisation of an object point process. The energy function of such a process can be written as follows:

$$U(\mathbf{y}|\theta) = U_{\mathbf{d}}(\mathbf{y}|\theta) + U_i(\mathbf{y}|\theta) \quad (3)$$

where $U_{\mathbf{d}}(\mathbf{y}|\theta)$ is the data energy and $U_i(\mathbf{y}|\theta)$ the interaction energy.

The estimator of the filamentary structure in a field of galaxies together with the parameter estimates are given by the configuration of objects minimising the total energy function of the system

$$\begin{aligned} (\hat{\mathbf{y}}, \hat{\theta}) &= \arg \max_{\Omega \times \Psi} p(\mathbf{y}, \theta) = \arg \max_{\Omega \times \Psi} p(\mathbf{y}|\theta)p(\theta) \\ &= \arg \min_{\Omega \times \Psi} \{U_{\mathbf{d}}(\mathbf{y}|\theta) + U_i(\mathbf{y}|\theta) - \log p(\theta)\} \end{aligned} \quad (4)$$

with Ψ the model parameters space.

The minimisation of the energy function can be performed by means of a simulated annealing algorithm (van Lieshout (1994); Stoica et al. (2005a)). This method iteratively samples from $p(\mathbf{y}, \theta)^{1/T}$ while slowly decreasing the temperature parameter T . When the system is frozen *i.e.* $T \rightarrow 0$, the simulated annealing samples uniformly on the sub-space of configurations minimising the energy function (3).

In this case, the solution obtained is not unique. Hence, it is legitimate to ask if an element of the pattern really belongs to the pattern, or if its presence is due to random effects (Stoica et al. (2005a)).

For compact regions $\mathcal{S} \subseteq \mathbb{R}^3$ of finite volume $0 \leq \nu(\mathcal{S}) < \infty$, we write the probability that an object from the pattern \mathbf{y} covers \mathcal{S} , as follows:

$$\mathbb{P} \left(\mathbf{1} \left\{ \sum_{i=1}^{n(\mathbf{Y})} \mathbf{1}\{\mathcal{S} \subseteq s(Y_i)\} > 0 \right\} \right) = \mathbb{E}_{(\mathbf{Y}, \Theta)} \mathbf{1} \left\{ \sum_{i=1}^{n(\mathbf{Y})} \mathbf{1}\{\mathcal{S} \subseteq s(Y_i)\} > 0 \right\} \quad (5)$$

The cover probability given by (5) can be approximated by its Monte Carlo counterpart:

$$\hat{\mathbb{P}} \left(\mathbf{1} \left\{ \sum_{i=1}^{n(\mathbf{Y})} \mathbf{1}\{\mathcal{S} \subseteq s(Y_i)\} > 0 \right\} \right) = \frac{1}{U} \sum_{u=1}^U \mathbf{1} \left\{ \sum_{i=1}^{n(\mathbf{Y}_u)} \mathbf{1}\{\mathcal{S} \subseteq s(Y_{ui})\} > 0 \right\} \quad (6)$$

where $\mathbf{Y}_1, \dots, \mathbf{Y}_U$ are obtained sampling from $p(\mathbf{y}, \theta)$. For the pattern \mathbf{Y}_u , the set with the corresponding objects is $\{Y_{ui}, i = 1, \dots, n(\mathbf{Y}(u))\}$.

The formula (5) can be seen as a tool for studying the average behaviour in terms of location and shape of the unknown pattern exhibited by the data.

There are different choices for the study of the average behaviour of the shape exhibited by the data. For instance, we may compute the probability that a given compact region would be covered by the union of the objects, or the probability that an object intersects the given region. We have discarded these alternatives because they would lead to an over-detection of the filamentary pattern, similar to morphological dilation, and hence to filaments which are too thick.

3. Bisous model applied to filamentary pattern detection

Detection of cosmic filaments using marked point processes was first performed on two-dimensional simulated data by Stoica et al. (2005b). The marked point process that was used throughout the mentioned work was the Candy model. This marked point process is able to simulate and detect two-dimensional linear networks. Clearly, for real data analysis, a three-dimensional model is needed.

In this paper, we use the Bisous model, which is an object point process built to model and analyse general three dimensional spatial patterns (Stoica et al. (2005a)). The spatial pattern is made of simple interacting objects or generating elements. The particular property of these objects is that they exhibit a finite number q of rigid extremity points $\{e_1, \dots, e_q\}$. Around each object y an attraction region $a(y)$ is defined. This attraction region is the disjoint union $a(y) = \cup_{u=1}^q b(e_u, r_a)$, where $b(e_u, r_a)$ is the ball of fixed radius r_a centred in e_u . Objects attract each other through their attraction region. If they attract each other, then they may get connected. Connectivity is a more complex interaction than attraction. We will show later in this paper that for instance, connectivity takes also into account the orientation between the main symmetry axes of the objects. The connected objects form the pattern. The object connected to the pattern by means of s extremity points is called s -connected. Among the interactions exhibited by the objects forming the pattern we enumerate connectivity, alignment and repulsion. They are to be defined later in the next section of the paper.

For a pattern \mathbf{y} the probability density of the Bisous model can be written as follows:

$$p(\mathbf{y}|\theta) \propto \left[\prod_{i=1}^{n(\mathbf{y})} \beta(y_i) \right] \left[\prod_{s=0}^q \gamma_s^{n_s(\mathbf{y})} \right] \prod_{\kappa \in \Gamma} \gamma_\kappa^{n_\kappa(\mathbf{y})} \quad (7)$$

where $\beta : K \times M \rightarrow \mathbb{R}_+$ is a positive function and $\gamma_s > 0, \gamma_\kappa \in [0, 1]$ are the interaction model parameters. The function $\beta(y)$ is defined below by $\log \beta(y) = u(y)$, where $u(y)$ is given by (10). Γ is a set of interactions between objects that are pairwise, local (distance based), symmetric and guarantee that the density (7) is well defined. For each s and κ the sufficient statistics $n_s(\mathbf{y})$ and $n_\kappa(\mathbf{y})$ represent, respectively, the number of s -connected objects and the number of pairs of objects exhibiting the interaction of type κ in the configuration \mathbf{y} .

The total energy of the model $U(\mathbf{y}|\theta)$ is computed taking the negative logarithm function of (7). We naturally define its two components, the data energy

$$U_d(\mathbf{y}|\theta) = - \sum_{i=1}^{n(\mathbf{y})} \log \beta(y_i) \quad (8)$$

and the interaction energy

$$U_i(\mathbf{y}|\theta) = - \sum_{s=0}^q n_s(\mathbf{y}) \log \gamma_s - \sum_{\kappa \in \Gamma} n_\kappa(\mathbf{y}) \log \gamma_\kappa. \quad (9)$$

In the following, we will present the generating element together with its corresponding interactions that define (9), and will define the data energy (8), which is related to the location of the filamentary pattern among the galaxies.

3.1. Generating element and its interactions

The generating element of the filamentary pattern “hidden” in the galaxy data is a random thin cylinder. Such a cylinder has a random centre in K and has a fixed radius r and a height h , with $r \ll h$. Its random mark is given by ω , the orientation vector of the cylinder. Its corresponding parameters $\omega = \phi(\eta, \tau)$ are uniformly distributed on $M = [0, 2\pi) \times [0, 1]$ such that

$$\omega = (\sqrt{1 - \tau^2} \cos(\eta), \sqrt{1 - \tau^2} \sin(\eta), \tau).$$

A cylinder (k, ω) has $q = 2$ extremity points. In Figure 2 the cylinder is centred in the origin and its symmetry axis is parallel to Oz . The coordinates of the extremity points are

$$e_u = (0, 0, (-1)^{u+1}(\frac{h}{2} + r_a)), \quad u \in \{1, 2\}$$

and the orientation vector is $\omega = (0, 0, 1)$. A randomly located and oriented cylinder is obtained by the means of a translation and two rotations (Hearn and Baker (1994)).

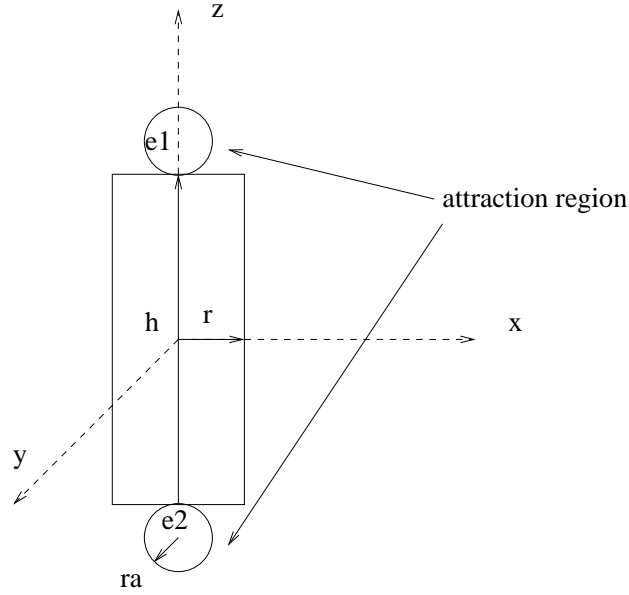


Fig. 2. Generating element for the filamentary pattern.

Two cylinders $y_1 = (k_1, \omega_1)$ and $y_2 = (k_2, \omega_2)$ attract each other, and we write $y_1 \sim_a y_2$ if the set

$$\{(u, v) : 1 \leq u, v \leq 2, u \neq v, d(e_u(y_1), e_v(y_2)) \leq r_a\}$$

contains only one element.

The same cylinders reject each other, and we write $y_1 \sim_r y_2$ if $d(k_1, k_2) < h$. They are aligned, and we write $y_1 \sim_{\parallel} y_2$ if

$$\omega_1 \cdot \omega_2 \geq 1 - \tau_{\parallel}$$

where $\tau_{\parallel} \in (0, 1)$ is a predefined curvature parameter and \cdot designs the scalar product of the two orientation vectors. If

$$|\omega_1 \cdot \omega_2| \leq \tau_{\perp}$$

where $\tau_{\perp} \in (0, 1)$ is a predefined crossing curvature, they are said to be orthogonal, and we write $y_1 \sim_{\perp} y_2$.

Two cylinders y_1 and y_2 are connected and we write $y_1 \sim_c y_2$ if the following conditions are simultaneously fulfilled:

$$\begin{aligned} y_1 &\sim_a y_2 \\ y_1 &\not\sim_r y_2 \\ y_1 &\sim_{\parallel} y_2 \end{aligned}$$

If the following conditions are simultaneously verified:

$$\begin{aligned} y_1 &\sim_r y_2 \\ y_1 &\not\sim_{\perp} y_2 \end{aligned}$$

the cylinders exhibit a hard repulsion, and we write $y_1 \sim_h y_2$.

The filaments forming the pattern are made of cylinders that attract each other and they are well aligned. These filaments may cross. At the same time configurations with overlapping cylinders are not desirable since they may outline clusters of galaxies instead of filaments.

In Figure 3 a cylinder configuration is represented in two dimensions. According to the previous definitions, we observe that $c_1 \sim_c c_2$ since $c_1 \sim_a c_2$, $c_1 \not\sim_r c_2$, and $c_1 \sim_{\parallel} c_2$. Thus, the cylinders c_1 and c_2 are s -connected. In order to form filaments, this kind of interaction is encouraged by the model. The cylinders c_2 and c_3 reject each other, but they are rather orthogonal, so their position is not penalised by the model. The cylinders c_2 and c_4 are not s -connected since $c_2 \not\sim_a c_4$, and their position is not encouraged nor penalised + by the model. The cylinders c_4 and c_5 reject each other, $c_4 \sim_r c_5$, and simultaneously they tend to overlap, $c_4 \not\sim_{\perp} c_5$. So, this pair of cylinders exhibits a hard repulsion interaction and this configuration is strongly penalised by the model.

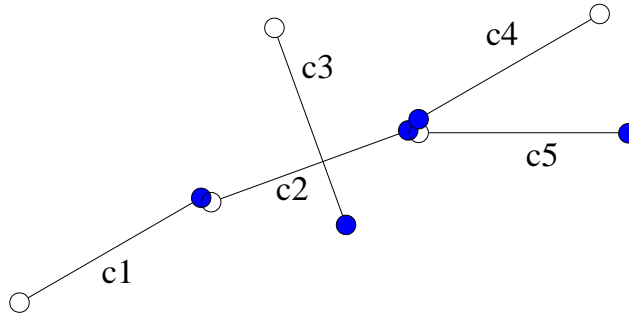


Fig. 3. Two-dimensional representation of a configuration of interacting cylinders.

With respect to these considerations, all the ingredients needed for the natural construction of the interaction energy (9) are defined. The s -connectivity is constructed using the relation \sim_c . The Γ set contains here only one element given by \sim_h . The model parameters for the interaction energy are $\gamma_0, \gamma_1, \gamma_2 > 0$ and $\gamma_h \in [0, 1]$. The definition of the interactions and the parameter ranges ensure the object point process induced by the interaction energy to be well defined, locally stable and Markov in the sense of Ripley-Kelly (Stoica et al. (2005a)).

3.2. The data energy

The data energy is related to the position of the filamentary pattern in the galaxy field. To each cylinder y an extra cylinder is attached, so that it has exactly the same parameters as y , except for the radius which equals $2r$. Let $\tilde{s}(y)$ be the shadow of $s(y)$ obtained by the subtraction of the initial cylinder from the extra cylinder, as indicated in Figure 4. The cylinder y is divided along its main symmetry axis, in three equal volumes, and we denote by $s_1(y)$, $s_2(y)$ and $s_3(y)$ their corresponding geometrical shapes.

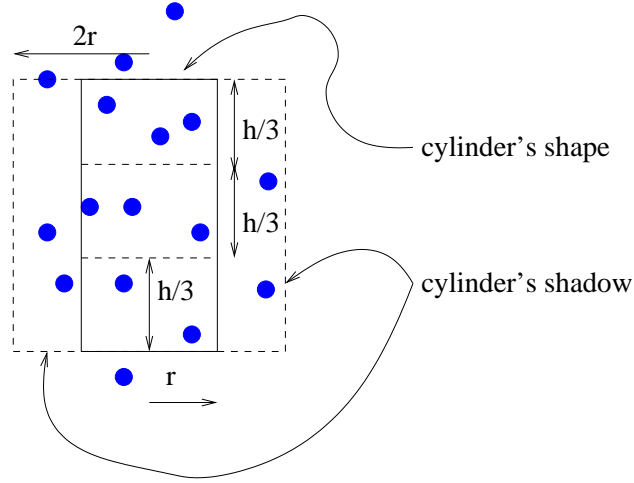


Fig. 4. A two-dimensional view of a cylinder with its shadow in a pattern of galaxies.

A cylinder may belong to the pattern if several conditions are verified. First, the density of galaxies inside $s(y)$ has to be higher than the density of galaxies in $\tilde{s}(y)$, and it can be written as follows:

$$\mathbf{1}\{\text{“density”}\} = \mathbf{1}\{n(\mathbf{d} \cap s(y))\nu(\tilde{s}(y)) > n(\mathbf{d} \cap \tilde{s}(y))\nu(s(y))\}$$

where $n(\mathbf{d} \cap s(y))$ and $n(\mathbf{d} \cap \tilde{s}(y))$ represent the number of galaxies covered by the cylinder and its shadow, and $\nu(s(y))$ and $\nu(\tilde{s}(y))$ are the volumes of the cylinder and its shadow, respectively. Next, the galaxies covered have to be spread inside the whole volume. This is formulated below:

$$\mathbf{1}\{\text{“spread”}\} = \prod_{i=1}^3 \mathbf{1}\{n(\mathbf{d} \cap s_i(y)) > 1\}$$

with $n(\mathbf{d} \cap s_i(y))$ the number of galaxies belonging to $s_i(y)$. Under these assumptions, $u(y)$ the energy contribution of a cylinder is defined as follows:

$$u(y) = \mathbf{1}\{\text{“density”}\} \mathbf{1}\{\text{“spread”}\} (n(\mathbf{d} \cap s(y)) - n(\mathbf{d} \cap \tilde{s}(y)) + u_{\max}) - u_{\max} \quad (10)$$

where u_{\max} is a positive fixed quantity. The introduction of this term gives to a segment that does not meet all the previous conditions, a very small chance to be a part of the network. This should give more complete networks and better mixing properties to the method.

The data energy (8) is obtained by summing the energy contributions (10) for all the cylinders in the pattern:

$$U_{\mathbf{d}}(\mathbf{y}|\theta) = - \sum_{i=1}^{n(\mathbf{y})} u(y_i). \quad (11)$$

It can be checked that the data energy term (11) induces a locally stable object point process.

4. Data

4.1. Observational data

The best available redshift catalogue to study morphology of the galaxy distribution at present is the 2dF Galaxy Redshift Survey (2dFGRS) (Colless et al., 2001). The catalogue covers two separate regions in the sky, the NGP (North Galactic Cap) strip, and the SGP (South Galactic Cap) strip, with total area of about 1500 square degrees. The nominal (extinction-corrected) magnitude limit of the catalogue is $b_j = 19.45$; reliable redshifts were obtained for 221414 galaxies. As seen in Fig. 1, the effective depth of the catalogue is about $z = 0.2$ or $D \approx 600 h^{-1}$ Mpc, and the total volume $V \approx 3.3 \cdot 10^7 h^{-3}$ Mpc³.

As all galaxy redshift catalogues, the catalogue is not strictly homogeneous. First, due to different observing conditions, the magnitude limit (the depth of the catalogue) changes from observation to observation, but the changes are known and well documented. Second, due to the fact that the fibers that lead the light from the focal plane to the spectrograph have a finite size, the redshifts of a few per cent of selected galaxies could not be measured. This effect is quantified as redshift completeness. All the data and the programs to calculate the magnitude limits and the spectroscopic completeness are public and can be found at <http://www.mso.anu.edu.au/2dFGRS/>.

The 2dFGRS catalogue is flux-limited catalogue and therefore the density of galaxies decreases with distance. For statistical analysis of such surveys, a weighting scheme that compensates for the missing galaxies at large distances, has to be used. Usually, each galaxy is weighted by the inverse of the selection function (Martínez and Saar, 2002). The selection function is determined by the two main selection effects described above. However, such a weighting is suitable only for specific statistical problems, as, e.g., the calculation of correlation functions. When studying the local structure, such a weighting cannot be used; it would only amplify the shot noise.

At the cost of discarding many surveyed galaxies, one can alternatively use volume-limited samples. In this case, the variation in density at different locations depends only on the fluctuations of the galaxy distribution itself. We started our analysis by using the volume-limited samples prepared by the 2dF team for scaling studies (Croton et al. (2004)) and kindly sent to us by Darren Croton. Unfortunately, we found soon that the galaxy density in these samples was too low and the shot noise did not allow algorithms to find filaments; there are, typically, only of the order of ten galaxies per filament in such samples.

Thus we choose another way – we started from a full galaxy sample, and choose from that bricks in a limited distance range, where the galaxy density was approximately constant. We use bricks in this paper to avoid problems with complex boundaries of the full 2dFGRS sample. As the SGP half of the galaxy sample has a convex geometry (it is limited by two conical sections of different opening angles), the constant density bricks that is possible to cut from the SGP have small volumes. Thus we used only the NGP data, and chose three

Table 1. Galaxy content and geometry for the 2dFGRS bricks (in $h^{-1}\text{Mpc}$). N_{gal} is the number of galaxies in a sample, D_{min} is the distance of a sample from the observer (its nearest point), D_{max} is the maximum distance in a sample from the observer (to the far-away brick corners) and d is the mean distance between galaxies in a sample.

sample	N_{gal}	D_{min}	depth	width	height	D_{max}	d
NGP150	2499	87.9	53.1	101.5	12.4	150.0	2.99
NGP200	4180	117.2	70.9	135.3	16.5	200.0	3.36
NGP250	7588	146.4	88.6	169.1	20.7	250.0	3.44

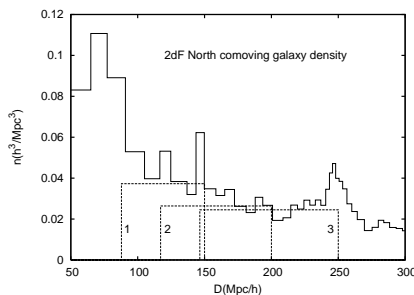


Fig. 5. Galaxy density for the full 2dFGRS NGP sample (in comoving coordinates) versus the distance D from the observer. As the nearby volume is small, single superclusters cause strong spikes in the histogram. The most prominent supercluster that creates the spike at $D \approx 250 h^{-1}\text{Mpc}$, lies just outside of the largest data brick used in this work.

bricks of maximum length and height, with different depths. General characteristics of these data sets are listed in Table 1. As seen from the (comoving) galaxy density histogram in Fig. 5, the densities inside the bricks are approximately constant.

We show one of these three bricks inside the 2dFGRS NGP sample limits and the spatial distribution of galaxies in Fig. 6.

4.2. Experimental results

As described above, we use three data sets, drawn from the galaxy distribution in the Northern subsample of the 2dFGRS survey. The size of the brick determines the size of K . As the data resolution is similar (column d in Table 1, we choose the same values for the dimensions of the cylinder for all the data sets, as follows: $r = 0.5$, $h = 6.0$. The radius of the cylinder is close to the minimal one can choose, taking into account the data resolution. Its height is also close to the shortest possible, as our shadow cylinder has to have a cylindrical geometry, too (the ratio of its height to the diameter is presently 3:1). We choose the attraction radius as $r_a = 0.5$, giving for the maximum distance between connected cylinders the value 1.5, and the pre-defined curvatures are $\tau_{\parallel} = \tau_{\perp} = 0.15$. This allows for a maximum of $\approx 30^\circ$ between the direction angles of connected cylinders, and limits the orthogonality condition to angles larger than $\approx 80^\circ$.

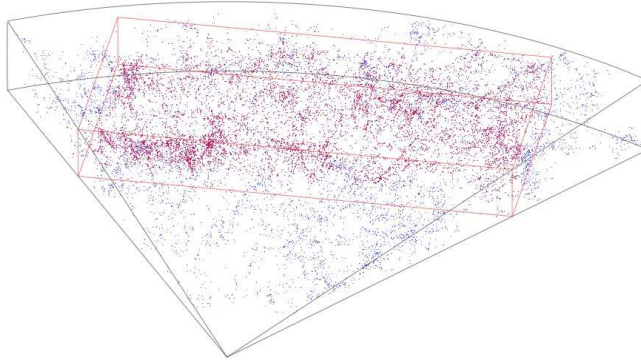


Fig. 6. One of the cuboidal samples analysed in this paper drawn from the Northern Galactic Cap of the 2dFGRS. The wedge shows the approximate extent of the full sample, its real borders are more complex.

The data energy parameter is $u_{\max} = -25$. For the interaction energy, the parameter domain is chosen as follows: $\log \gamma_0 \in [-12.5, -7.5]$, $\log \gamma_1 \in [-5, 0]$ and $\log \gamma_2 \in [0, 5]$. The hard repulsion parameter is $\gamma_h = 0$, so the configurations with cylinders exhibiting such interactions are forbidden. The domain of the connection parameters was chosen such that 2-connected cylinders are generally encouraged, 1-connected cylinders are penalised and 0-connected segments are strongly penalised. This choice encourages the cylinders to group in filaments in those regions where the data energy is good enough. Still, we have no information about the relative strength of those parameters. Therefore, we have decided to use for the prior parameter density $p(\theta)$ the uniform law over the parameter domain.

A delicate point when building a simulated annealing procedure is the choice of an appropriate cooling schedule for the temperature. (Stoica et al. (2005a)) proved that the use of a logarithmic cooling schedule guarantees the convergence of the simulated annealing algorithm when the parameters of the point process are fixed. Therefore, we have chosen the following scheme for the descent of the temperature:

$$T_n = \frac{T_0}{1 + \log n}$$

with $T_0 = 1$.

We ran the simulated annealing algorithm for 250000 iterations. Samples were picked up every 250 iterations. The obtained cylinder configurations for the data sets *NGP150*, *NGP200* and *NGP250* are shown in Figure 7b, Figure 8b and Figure 9b, respectively.

The cylinders obtained after running the simulated annealing are situated in the regions where we see that the data exhibit filamentary structures. Still, as simulated annealing requires infinitely many iterations till convergence, and also because of the fact that an infinity of solutions are proposed, we shall use coverage probabilities to “average” the shape of the filaments.

For each data set the corresponding domain K was divided into small cubic cells of size $1 h^{-1}\text{Mpc}$. These cells are small enough to be covered by a single cylinder. Computing the coverage probabilities directly using simulating annealing outputs is not possible since (6)

Table 2. The mean of the sufficient statistics for the three data sets: \bar{n}_2 is the mean number of the 2-connected cylinders, \bar{n}_1 is the mean number of the 1-connected cylinders and \bar{n}_0 is the mean number of the 0-connected cylinders.

Sufficient statistics	Data sets		
	NGP150	NGP200	NGP250
\bar{n}_2	4.13	5.83	9.88
\bar{n}_0	15.88	21.19	35.82
\bar{n}_1	21.35	35.58	46.49

is an expectation under $p(\mathbf{y}, \theta)$. Hence, the algorithm was run until T_0 , a fixed temperature close to zero, was reached. The coverage probabilities were computed as an expectation similar to (6) but under the law given by $p(\mathbf{y}, \theta)^{1/T_0}$. The obtained result was thresholded using three distinct values: 0.5, 0.75 and 0.95. For each of these values we obtain a map of the cells that have been visited by our model with a frequency higher or equal than the given value. These visit maps for the data sets *NGP150*, *NGP200* and *NGP250* are shown in Figure 7c-d, Figure 8c-d and Figure 9c-d respectively.

The filamentary network is clearly outlined. Here we consider a filament the geometric structure obtained recursively from a visited cell and its corresponding neighbouring cells. In this case, we have defined the neighbours of a cell, the cells that have coordinates incremented or decremented by one with respect to the reference cell. Hence, a cell has 26 neighbouring cells.

Although many filaments are of simple form, there are many filaments which exhibit complex morphology, from simple branching to multibranch complexes. This is a new fact that will probably force cosmologists to reconsider their usual notion of filaments as simple bridges between clusters of galaxies. We show two examples of such filaments below, one of a comparatively simple shape (Fig. 10), and another of very complex shape (Fig. 11).

4.3. Statistics

The coverage probabilities are not a global test for our method, because these probabilities are computed only for small regions. The computation of the probability that a whole filament is covered by our model requires the knowledge a priori of the shape of the filament. (Stoica et al. (2005a)) used for a different problem – cluster detection in epidemiological data – a test, to check that the pattern is detected rather because of the data than of the model parameters.

Following this idea, the following experiments were carried out for each data set. First, the method was launched during 50000 iterations at fixed $T = 1.0$. Samples were picked up every 250 iterations. The means of the sufficient statistics of the model were computed using these samples. The obtained results are shown in Table 2.

The second experiment consisted of re-distributing uniformly the points inside the domain K . So, the points follow a binomial distribution. For each data set this operation was done 100 times, hence obtaining 100 point fields. For each point field the method was launched in the conditions previously described. The mean of the sufficient statistics was then computed. The maximum values over all the 100 means for each data set are shown in Table 3.

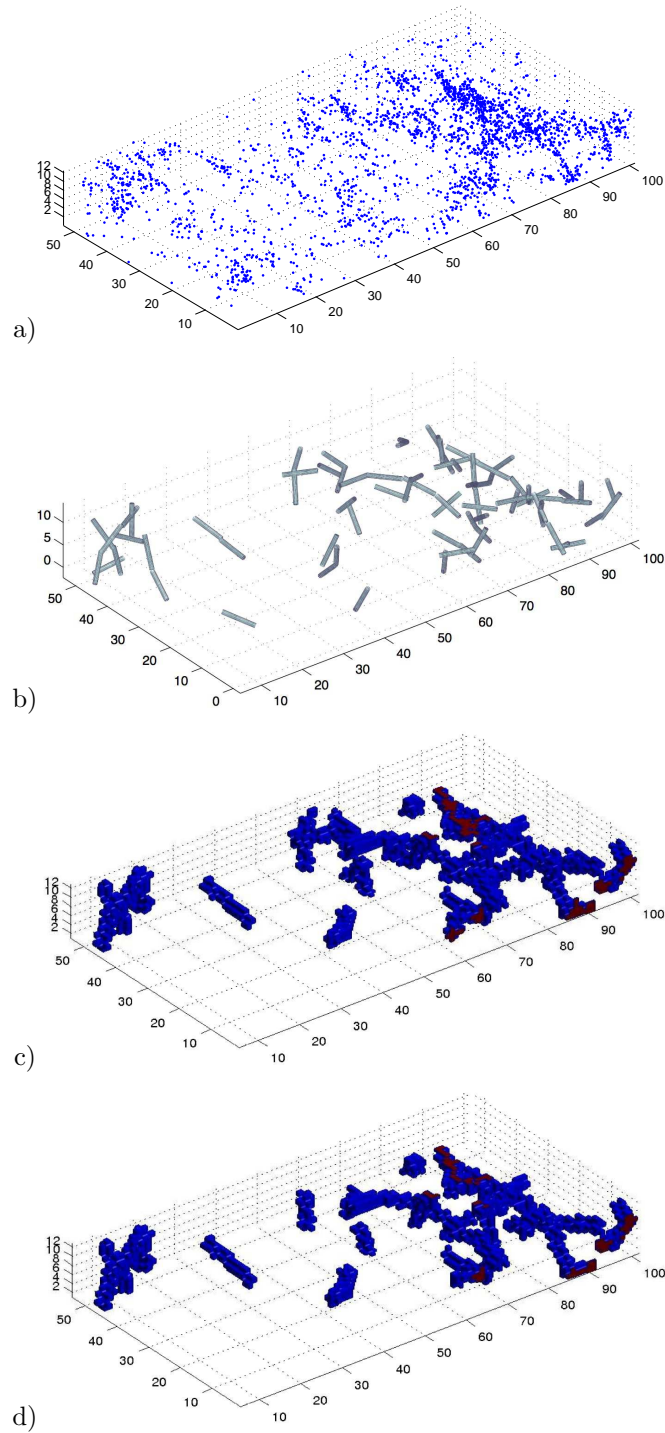


Fig. 7. Data set *NGP150*. a) The data. b) Cylinder configuration obtained using the simulated annealing algorithm. Cover probabilities thresholded at c) 50%, d) 95%.

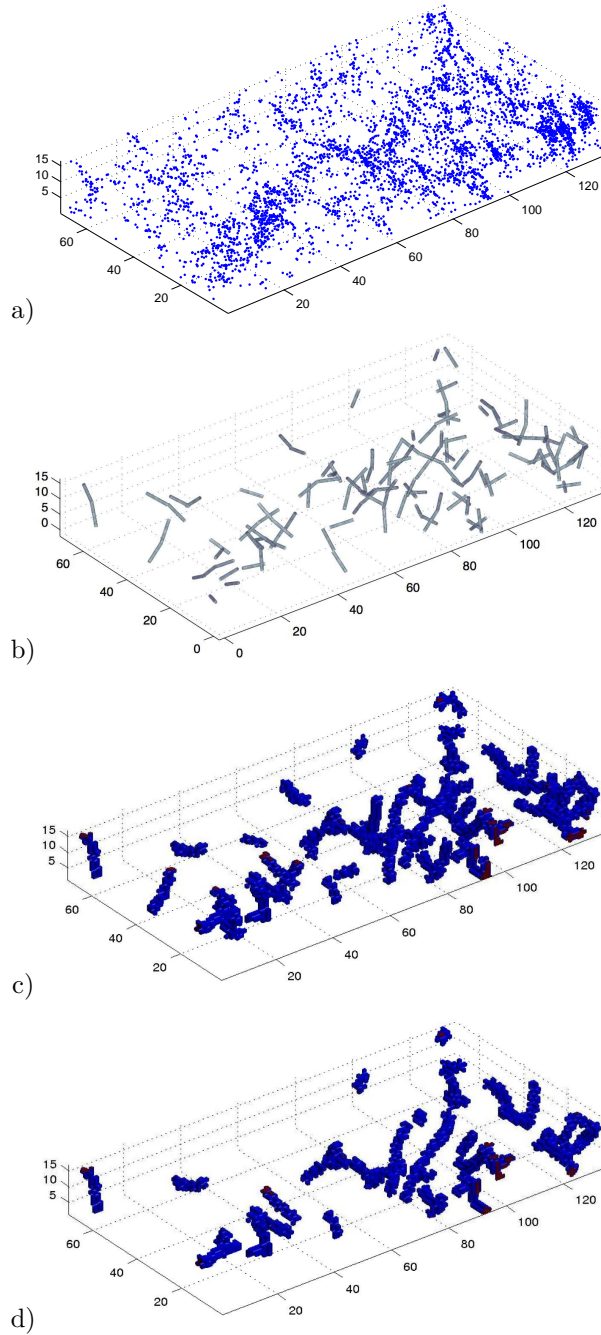


Fig. 8. Data set *NGP200*. a) The data, b) Cylinder configuration obtained using the simulated annealing algorithm. Cover probabilities thresholded at c) 50%, d) 95%.

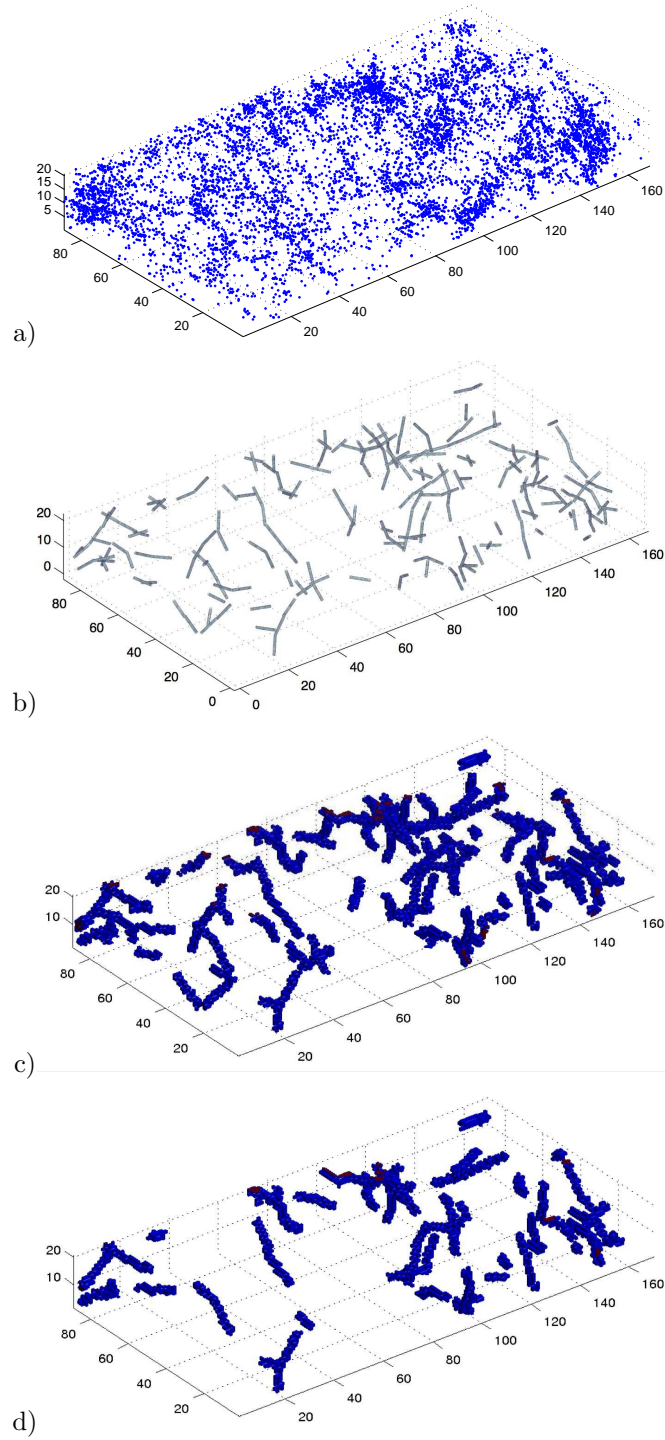


Fig. 9. Data set *NGP250*. a) The data, b) Cylinder configuration obtained using the simulated annealing algorithm. Cover probabilities thresholded at c) 50%, d) 95%.

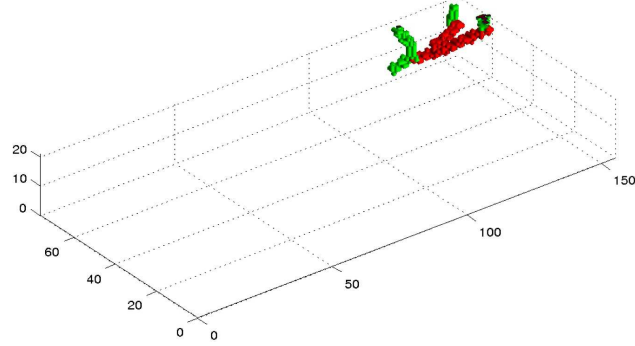


Fig. 10. A simple filament from the *NGP250* sample. Lighter shading (green colour) shows the 50% cover probability threshold, darker shading (red colour) – the 95% threshold.

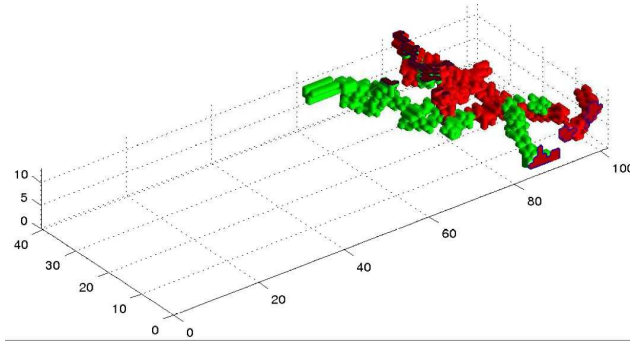


Fig. 11. A complex filament from the *NGP150* sample. Lighter shading (green colour) shows the 50% cover probability threshold, darker shading (red colour) – the 95% threshold.

Table 3. The maximum of mean of the sufficient statistics over binomial fields generated for each of the three data sets: $\max \bar{n}_2$ is the maximum mean number of the 2-connected cylinders, $\max \bar{n}_1$ is the maximum mean number of the 1-connected cylinders and $\max \bar{n}_0$ is the maximum mean number of the 0-connected cylinders.

Sufficient statistics	Binomial data sets		
	NGP150	NGP200	NGP250
$\max \bar{n}_2$	0.015	0.05	0.015
$\max \bar{n}_0$	0.54	0.27	0.45
$\max \bar{n}_1$	0.39	0.24	0.33

These results clearly indicate that the original data exhibit a filamentary structure. No filamentary structure is detected when the same model runs over binomial fields of points that has the same number of points as the original data. This test discriminates the two cases at a p -value less than 1%, and assures us that the filaments we find are due to data and not to our model.

5. Conclusion and perspectives

We have applied an object point process – Bisous model – to objectively find filaments in galaxy redshift surveys (three-dimensional galaxy maps). For that, we defined the model, fixed some of the interaction parameters and chose priors for the remaining parameters. The definition of the data term is very intuitive and rather a simple test. Much more elaborated methods testing the alignment of the points along the direction of the cylinder against the completely spatial randomness need investigation. The uniform law for the interaction parameters was preferred in order to give the same chances to a wide range of topologies of the filamentary network. Still, if concrete prior information about the topology of the filamentary network is available then this should be integrated in the model.

We have run simulated annealing sequences and select filaments on the basis of coverage probabilities for individual cells of sample volume. The coverage probabilities are to be seen as a way of averaging the shape of the filamentary structure. They have the advantage to allow inference from statistics instead of a single realisation. Their main drawback is that the coverage probabilities are computed locally, for small regions. Still, the visualisation of the visit maps built on these probabilities brings new ideas and hypotheses about the topologies of the cosmic filaments. A global Monte Carlo statistical test was built to test the existence of the filaments in the data. To do this, we have calculated sufficient statistics for the data sets and made a comparison with the sufficient statistics obtained on binomial point fields having the same number of points as the data. Our test was indicating that the filaments we find are defined by the data, not by the chosen model.

The method used in this paper can be extended in different ways. One natural extension is to use different generating elements instead on cylinders, e.g., planar elements or clusters. (Stoica et al. (2005a)). Although traces of planar structures are seen in superclusters of galaxies, these have been difficult to quantify, mainly because of their low density contrast. Another interesting application is to search for dynamically bound groups and clusters of galaxies that have a typical 'finger-of-God' signature in redshift space, extended along the line-of-sight. And there remains a question if the method could be extended to inhomogeneous point processes – this would allow us to use all the observational data, not only volume-limited subsamples.

6. Acknowledgements

We thank our referees for their thorough analysis and constructive comments. This work has been supported by the University of Valencia through a visiting professorship for Enn Saar, by the Spanish MCyT project AYA2003-08739-C02-01 (including FEDER) and AYA2006-14056, by the Estonian Ministry of Education and Science, research project TO 0062465s03, and by the Estonian Science Foundation grant 6104.

References

- Barrow, J. D., D. H. Sonoda, and S. P. Bhavsar (1985). Minimal spanning tree, filaments and galaxy clustering. *Monthly Notices of the Royal Astronomical Society* 216, 17–35.
- Berthelsen, K. K. and J. Møller (2002). A primer on perfect simulation for spatial point processes. *Bulletin of the Brazilian Mathematical Society* 33, 351–367.
- Bharadwaj, S., S. P. Bhavsar, and J. V. Sheth (2004). The size of the longest filaments in the universe. *The Astrophysical Journal* 606, 25–31.
- Bharadwaj, S. and B. Pandey (2004, November). Using the Filaments in the Las Campanas Redshift Survey to Test the Λ CDM Model. *The Astrophysical Journal* 615, 1–6.
- Colberg, J. M., K. S. Krughoff, and A. J. Connolly (2005, May). Intercluster filaments in a Λ CDM Universe. *Monthly Notices of the Royal Astronomical Society* 359, 272–282.
- Colless, M., G. Dalton, S. Maddox, W. Sutherland, P. Norberg, S. Cole, J. Bland-Hawthorn, T. Bridges, R. Cannon, C. Collins, W. Couch, N. Cross, K. Deeley, R. De Propris, S. P. Driver, G. Efstathiou, R. S. Ellis, C. S. Frenk, K. Glazebrook, C. Jackson, O. Lahav, I. Lewis, S. Lumsden, D. Madgwick, J. A. Peacock, B. A. Peterson, I. Price, M. Seaborne, and K. Taylor (2001, December). The 2dF Galaxy Redshift Survey: spectra and redshifts. *Monthly Notices of the Royal Astronomical Society* 328, 1039–1063.
- Croton, D. J., M. Colless, E. Gaztañaga, C. M. Baugh, P. Norberg, I. K. Baldry, J. Bland-Hawthorn, T. Bridges, R. Cannon, S. Cole, C. Collins, W. Couch, G. Dalton, R. de Propris, S. P. Driver, G. Efstathiou, R. S. Ellis, C. S. Frenk, K. Glazebrook, C. Jackson, O. Lahav, I. Lewis, S. Lumsden, S. Maddox, D. Madgwick, J. A. Peacock, B. A. Peterson, W. Sutherland, and K. Taylor (2004, August). The 2dF Galaxy Redshift Survey: voids and hierarchical scaling models. *Monthly Notices of the Royal Astronomical Society* 352, 828–836.
- Eriksen, H. K., D. I. Novikov, P. B. Lilje, A. J. Banday, and K. M. Górski (2004, September). Testing for Non-Gaussianity in the Wilkinson Microwave Anisotropy Probe Data: Minkowski Functionals and the Length of the Skeleton. *The Astrophysical Journal* 612, 64–80.
- Geyer, C. J. (1994). On the convergence of monte carlo maximum likelihood calculations. *Journal of the Royal Statistical Society, Series B* 56, 261–274.
- Geyer, C. J. (1999). Likelihood inference for spatial point processes. In O. Barndorff-Nielsen, W. S. Kendall, and M. N. M. van Lieshout (Eds.), *Stochastic geometry, likelihood and computation*. CRC Press/Chapman and Hall, Boca Raton.
- Geyer, C. J. and J. Møller (1994). Simulation procedures and likelihood inference for spatial point processes. *Scan. J. Stat.* 21, 359–373.
- Geyer, C. J. and E. A. Thompson (1992). Constrained monte carlo maximum likelihood for dependent data. *Journal of the Royal Statistical Society, Series B* 54, 657–699.
- Green, P. (1995). Reversible jump MCMC computation and bayesian model determination. *Biometrika* 82, 711–732.

- Hearn, D. and M. P. Baker (1994). *Computer graphics. Second edition*. Prentice-Hall, Englewood Cliffs, NJ.
- Kendall, W. S. and J. Møller (2000). Perfect simulation using dominating processes on ordered spaces, with application to locally stable point processes. *Adv. Appl. Prob.* *32*, 844–865.
- Lacoste, C., X. Descombes, and J. Zerubia (2005). Point processes for unsupervised line network extraction in remote sensing. *IEEE Trans. Pattern Analysis and Machine Intelligence*, *27*, 1568–1579.
- Martínez, V. J. and E. Saar (2002). *Statistics of the Galaxy Distribution*. Chapman & Hall/CRC, Boca Raton.
- Møller, J., A. N. Pettitt, K. K. Berthelsen, and R. W. Reeves (2004). An efficient markov chain monte carlo method for distributions with intractable normalizing constants. Research report R-2004-02, Department of Mathematical Sciences, Aalborg University.
- Møller, J. and R. P. Waagepetersen (2003). *Statistical inference for spatial point processes*. Chapman & Hall/CRC, Boca Raton.
- Novikov, D., S. Colombi, and O. Doré (2006). Skeleton as a probe of the cosmic web: the two-dimensional case. *Monthly Notices of the Royal Astronomical Society* *366*, 1201–1216.
- Pandey, B. and S. Bharadwaj (2005, March). A two-dimensional analysis of percolation and filamentarity in the Sloan Digital Sky Survey Data Release One. *Monthly Notices of the Royal Astronomical Society* *357*, 1068–1076.
- Pimblet, K. A. (2005). Pulling Out Threads from the Cosmic Tapestry: Defining Filaments of Galaxies. *Publications of the Astronomical Society of Australia* *22*, 136–143.
- Pimblet, K. A. and M. J. Drinkwater (2004, January). Intercluster Filaments of Galaxies Programme: pilot study survey and results. *Monthly Notices of the Royal Astronomical Society* *347*, 137–143.
- Pimblet, K. A., M. J. Drinkwater, and M. C. Hawkrigg (2004, November). Intercluster filaments of galaxies programme: abundance and distribution of filaments in the 2dFGRS catalogue. *Monthly Notices of the Royal Astronomical Society* *354*, L61.
- Preston, C. J. (1977). Spatial birth-and-death processes. *Bull. Int. Stat. Inst.* *46*, 371–391.
- Reiss, R. D. (1993). *A course on point processes*. Springer-Verlag, New York.
- Sousbie, T., C. Pichon, H. Courtois, S. Colombi, and D. Novikov (2006). The 3D skeleton of the SDSS. *astro-ph/0602628*.
- Stoica, R. S., X. Descombes, M. N. M. van Lieshout, and J. Zerubia (2002). An application of marked point processes to the extraction of linear networks from images. In J. Mateu and F. Montes (Eds.), *Spatial statistics through applications*. WIT Press, Southampton, UK.
- Stoica, R. S., X. Descombes, and J. Zerubia (2004). A Gibbs point process for road extraction in remotely sensed images. *Int. J. Computer Vision* *57(2)*, 121–136.

- Stoica, R. S. and E. Gay (2005, July). Cluster detection in spatial data using marked point processes. Research report 11-2005, INRA, Avignon.
- Stoica, R. S., P. Gregori, and J. Mateu (2005a). Simulated annealing and object point processes : tools for analysis of spatial patterns. *Stochastic Processes and their Applications* 115, 1860–1882.
- Stoica, R. S., V. J. Martinez, J. Mateu, and E. Saar (2005b). Detection of cosmic filaments using the Candy model. *Astronomy and Astrophysics* 434, 423–432.
- van Lieshout, M. N. M. (1994). Stochastic annealing for nearest-neighbour point processes with application to object recognition. *Adv. Appl. Prob.* 26, 281–300.
- van Lieshout, M. N. M. (2000). *Markov point processes and their applications*. Imperial College Press/World Scientific Publishing, London/Singapore.
- van Lieshout, M. N. M. and R. S. Stoica (2003a). The Candy model revisited: properties and inference. *Stat. Neerlandica* 57, 1–30.
- van Lieshout, M. N. M. and R. S. Stoica (2003b). Perfect simulation for marked point processes. Research report PNA-0306, CWI.
- van Lieshout, M. N. M. and R. S. Stoica (2006). Perfect simulation for marked point processes. *Computational Statistics and Data Analysis* 51, 679–698.